ARTICLE

Composite Cathode Based on Redox-Reversible Nb_2TiO_7 for Direct High-Temperature Steam Electrolysis

Shi-song Li, Ji-gui Cheng*, Xu-cheng Zhang, Yu Wang, Kui Xie*

Department of Energy Materials, School of Materials Science and Engineering, Hefei University of Technology, Hefei 230009, China

(Dated: Received on December 18, 2014; Accepted on March 24, 2015)

Ni/YSZ fuel electrodes can only operate under strongly reducing conditions for steam electrolysis in an oxide-ion-conducting solid oxide electrolyzer (SOE). In atmosphere with a low content of H_2 or without H_2, cathodes based on redox-reversible Nb_2TiO_7 provide a promising alternative. The reversible changes between oxidized Nb_2TiO_7 and reduced $Nb_{1.33}Ti_{0.67}O_4$ samples are systematically investigated after redox-cycling tests. The conductivities of Nb_2TiO_7 and reduced $Nb_{1.33}Ti_{0.67}O_4$ are studied as a function of temperature and oxygen partial pressure and correlated with the electrochemical properties of the composite electrodes in a symmetric cell and SOE at 830 °C. Steam electrolysis is then performed using an oxide-ion-conducting SOE based on a $Nb_{1.33}Ti_{0.67}O_4$ composite fuel electrode at 830 °C. The current-voltage and impedance spectroscopy tests demonstrate that the reduction and activation of the fuel electrode is the main process at low voltage; however, the steam electrolysis dominates the entire process at high voltages. The Faradic efficiencies of steam electrolysis reach 98.9% when $3\%H_2O/Ar/4\%H_2$ is introduced to the fuel electrode and 89% for that with introduction of $3\%H_2O/Ar$.

Key words: Redox-reversible, Alternative fuel electrode, Solid oxide electrolyzer, Steam electrolysis

I. INTRODUCTION

Hydrogen attracts particular interest because it has the potential to be created using renewable resources, stored, and transported, and it is an environmentally friendly source of energy [1−4]. Natural gas reforming is currently the main technique for massive hydrogen production; however, this process still relies on fossil fuel consumption. Water electrolysis capable of producing hydrogen remains far from real application because of the large electricity consumption necessary for water splitting [5]. In contrast, steam electrolysis ($H_2O \rightarrow H_2+1/2O_2$) is promising as the high-temperature heat partly offers the energy for steam dissociation and then leads to favorable kinetics and thermodynamics [6−10].

Oxide-ion-conducting high-temperature solid oxide electrolyzers (SOEs), as the inverse of oxide-ion-conducting solid oxide fuel cells (SOFCs), have attracted substantial interest because they directly convert electrical energy into chemical energy [11−14]. These devices can efficiently produce hydrogen electrochemically through high-temperature steam electrolysis using renewable electricity. In this process, steam is split into hydrogen and oxide ions under an external electrolysis potential, while the oxide ions diffuse across the oxide-ion-conducting electrolyte to the oxygen electrode, where the formation of oxygen from oxide ions occurs in the three-phase boundary.

Ni/YSZ cermet, the currently preferred cathode material for high-temperature SOEs, requires a significant concentration of H_2 flowing over it to avoid the oxidation of Ni to NiO. The oxidation of Ni by steam not only leads to the loss of electrical conductivity in the fuel electrode but also produces large thermal expansion that adversely results in the delamination of fuel electrode layers from the electrolyte. It is therefore necessary to develop a redox-stable or redox-reversible ceramic fuel electrode for steam electrolysis with a low content of H_2 or even without H_2. Perovskite $La_xSr_{1-x}Cr_yMn_{1-y}O_{3-\delta}$ (LSCM) has been reported to be an active and redox-stable material that has attracted significant attentions in the field of fuel electrodes for high-temperature solid oxide fuel cells and SOEs [11, 15−17]. Direct steam electrolysis without the flow of reducing gas over the fuel electrode was recently demonstrated by Irvine *et al.* [11]. However, the p-type conduction mechanism of the LSCM was not ideally adapted to the strong reducing potential that leads to a large electrode polarization resistance [18−20]. In contrast to LSCM, $La_xSr_{1-x}TiO_{3+\delta}$ (LSTO) is an active, redox-stable material but exhibits high n-type conduc-

*Authors to whom correspondence should be addressed. E-mail: xiekui@hfut.edu.cn, jgcheng63@sina.com

tivity upon reduction and has been considered a breakthrough in redox-stable cathode materials for SOEs [13, 21, 22]. We have recently demonstrated that a composite fuel electrode based on LSTO is capable of performing direct steam electrolysis without flowing reducing gas over the fuel electrode [13]. However, the Faradic efficiency is not yet comparable to that of a traditional fuel electrode based on Ni metal as the electrocatalytic properties of these ceramic fuel electrodes are not sufficient for electrochemical steam reduction.

Solid oxide Nb_2TiO_7 is a monoclinic layered structure compound with the C2/m space group. After being reduced, the Nb_2TiO_7 transforms into the highly conductive oxide $Nb_{1.33}Ti_{0.67}O_4$ with tetragonal (P42/mnm) space group. The $Nb_{1.33}Ti_{0.67}O_4$ is a mixed conductor because of the edge sharing of NbO_6 octahedra along the *c*-axis, producing Nb−Nb metal bond overlap with an intermetallic distance of 3 Å. This high electronic conductivity is facilitated by the edge-sharing octahedra along the *c*-axis [23]. The high electronic conductivity and catalytic-active Nb^{4+} or Ti^{3+} in reduced $Nb_{1.33}Ti_{0.67}O_4$ are expected to provide electrocatalytic activity for direct steam splitting based on a $Nb_{1.33}Ti_{0.67}O_4$ cathode. However, oxidized Nb_2TiO_7 can be repeatedly obtained if the reduced $Nb_{1.33}Ti_{0.67}O_4$ is treated in an oxidizing atmosphere, which would offer redox-reversible transformations with promising possibilities to enhance the cycling performances of the SOE cathode.

In this work, Nb_2TiO_7 is synthesized by a solid-state reaction method and $Nb_{1.33}Ti_{0.67}O_4$ is obtained by reduction of the Nb_2TiO_7 sample. The electrical properties of the Nb_2TiO_7 and $Nb_{1.33}Ti_{0.67}O_4$ ceramics are symmetrically investigated and further correlated to the electrochemical performance of the composite fuel electrodes. Steam electrolysis is then performed in an oxide-ion-conducting SOE based on a $Nb_{1.33}Ti_{0.67}O_4$ composite fuel electrode with and without the flow of reducing gas over the fuel electrodes.

II. EXPERIMENTS

The Nb_2TiO_7 powder was synthesized by a solid-state reaction method using a stoichiometric amount of high-purity Nb_2O_5 and TiO_2, which were mixed and ground with acetone. The mixture was dried and pressed into pellets followed by firing at 1400 °C for 10 h in air. The pellets were then ground, repelletized, and fired at the same temperature for 10 h in air. The Nb_2TiO_7 sample was reduced at 830 °C in H_2 for 10 h to achieve a reduced form of the sample, $Nb_{1.33}Ti_{0.67}O_4$. The reduction-oxidation cycles of the Nb_2TiO_7 sample were performed at 830 °C for 10 h under reduced and oxidation atmospheres. The $Ce_{0.8}Sm_{0.2}O_{2-\delta}$ (SDC) powder was prepared by a combustion method using Sm_2O_3 and $Ce(NO_3)_4{\cdot}6H_2O$ followed by a heat treatment at 800 °C for 2 h in air [24]. These chemicals (chemical grade) were purchased from Sinopharm Chemical Reagent Co., Ltd. (China). X-ray diffraction (XRD, 2θ=3°/min, D/MAX2500V, Rigaku Corporation, Japan) measurements were performed on both oxides, reduced after redox cycles, of Nb_2TiO_7 and $Nb_{1.33}Ti_{0.67}O_4$. The valence state of the elements in Nb_2TiO_7 and $Nb_{1.33}Ti_{0.67}O_4$ was analyzed by X-ray photoelectron spectroscopy using an ESCALAB250 spectrometer with an Al Kα (1486.6 eV) radiation source.

Appropriate amounts of the Nb_2TiO_7 powders were pressed into bars followed by a heat treatment at 1400 °C for 10 h. The relative density of the bars reached approximately 81%. Then, a bar was reduced completely at 830 °C for 15 h in a pure H_2 atmosphere to obtain the $Nb_{1.33}Ti_{0.67}O_4$ bar sample. Conductivity tests of the Nb_2TiO_7 sample were performed in air using the dc four-terminal method from room temperature to 800 °C, and the conductivity was recorded as a function of temperature with an online system with a step size of 0.4 °C. The relationship between the conductivity and oxygen partial pressure was analyzed at 800 °C with the oxygen partial pressure ranging from 10^{-20} atm to 0.2 atm, which was adjusted by flowing 5%H_2/95%Ar at a flow rate of 20 mL/min. The conductivity tests for $Nb_{1.33}Ti_{0.67}O_4$ were performed in a reducing atmosphere (5%H_2/Ar) from room temperature to 800 °C, and the conductivity was recorded as a function of temperature with an online system with a step size of 0.4 °C. The relationship between the conductivity and oxygen partial pressure was examined at 800 °C with the oxygen partial pressure ranging from 10^{-20} atm to 0.2 atm, which was adjusted by flowing air at a flow rate of 0.5 mL/min to increase the oxygen partial pressure after stopping the flow of 5%H_2/Ar. The oxygen partial pressure and conductivity were recorded with an online oxygen sensor (Type 1231, ZrO_2-based oxygen sensor, Noveltech, Australia) and an online multi-meter (Keithley 2000, Digital Multimeter, Keithley Instruments. Inc., USA).

A 2-mm-thick YSZ disc electrolyte support was prepared by dry-pressing the YSZ powders into a green disk with a diameter of 20 mm and was then sintered at 1500 °C for 10 h. The composite oxygen electrode slurry was prepared by milling $La_{0.8}Sr_{0.2}MnO_3$ (LSM) with SDC (65:35 in weight ratio) in α-terpineol with an appropriate amount of cellulose additive. Similarly, the composite fuel electrode slurry was prepared using Nb_2TiO_7 and SDC (65:35 in weight ratio) by the method described above. The configurations of the symmetric solid oxide cell and SOE are NTO-SDC/YSZ/NTO-SDC and NTO-SDC/YSZ/LSM-SDC, respectively, and the two surfaces of the electrolyte were coated with an electrode slurry in symmetric positions with an area of 1 cm^2 followed by a heat treatment at 1100 °C for 3 h in air. The current collection layer was made with silver paste (SS-8060, Xinluyi, Shanghai, China), which was printed onto both electrode surfaces

DOI:10.1063/1674-0068/28/cjcp1412210

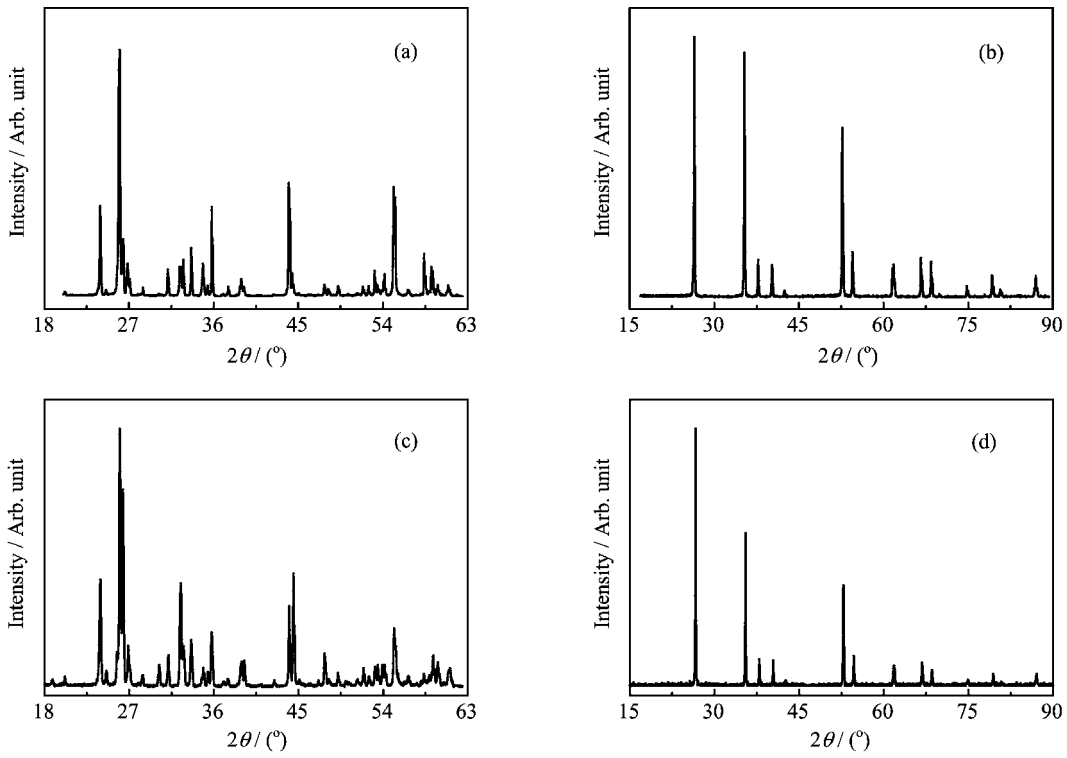

FIG. 1 XRD patterns of (a) Nb_2TiO_7 prepared by a solid-state reaction at 1400 °C, (b) $Nb_{1.33}Ti_{0.67}O_4$ prepared by reducing Nb_2TiO_7 at 830 °C in H_2 for 10 h, (c) and (d) Nb_2TiO_7 and $Nb_{1.33}Ti_{0.67}O_4$ after 3 reduction-oxidation cycles, respectively.

of the symmetric cell and electrolyzer. The external circuit consisted of silver electrical wire (0.1 mm in diameter), which was then connected to both current collectors using silver paste (DAD87, Shanghai Research Institute for Synthetic Resins) followed by firing at 550 °C (3 °C/min) for 30 min in air. The AC impendence of the symmetric solid oxide cell was tested at 830 °C with two electrodes exposed to pure H_2 under different passing current densities and tested in different H_2 partial pressures at the open-circuit voltage (OCV) condition.

The SOE with the configuration of NTO-SDC/YSZ/LSM-SDC was sealed onto homemade testing jigs using ceramic paste (JD-767, Jiudian, Dongguan, China) for electrochemical measurements. Before the tests, the composite fuel electrode (NTO-SDC) was reduced at 830 °C in H_2 atmosphere for 1 h to obtain the reduced electrode ($Nb_{1.33}Ti_{0.67}O_4$-SDC). The electrolyzer was typically tested at 830 °C with 3%H_2O/Ar/4%H_2 at a flow rate of 30 mL/min fed into the fuel electrode (NTO-SDC). The AC impedances of the SOE were measured with different applied voltages using an electrochemical workstation (IM6, Zahner, Germany). The current-voltage (I-V) and short-term performance under an external applied load were evaluated at 830 °C. The gas flow rate was controlled with a mass flow meter (D08-3F, Sevenstar, Beijing, China), and the hydrogen product was detected with an online gas chromatograph (GC9750II, Fuli, China).

III. RESULTS AND DISCUSSION

Figure 1 (a) and (b) present the XRD patterns of the oxide Nb_2TiO_7 and reduced sample $Nb_{1.33}Ti_{0.67}O_4$, which confirm the single phases of the Nb_2TiO_7 (PDF No.039-1407) and $Nb_{1.33}Ti_{0.67}O_4$ (PDF No.053-0293), respectively. The structure of Nb_2TiO_7 is monoclinic with space group of C2/m, and the structure of $Nb_{1.33}Ti_{0.67}O_4$ is tetragonal with space group of p42/mnm. Nb_2TiO_7 has unit-cell dimensions of a=1.768336 nm, b=0.380266 nm, and c=1.18969 nm, whereas $Nb_{1.33}Ti_{0.67}O_4$ has unit-cell dimensions of a=b=0.47626 nm and c=0.29989 nm. The decrease of volume is about 23.1% when Nb_2TiO_7 is reduced to $Nb_{1.33}Ti_{0.67}O_4$, which is much lower than that of NiO (about 40% when it is reduced). This result demonstrates that Nb_2TiO_7 or $Nb_{1.33}Ti_{0.67}O_4$ as a composite fuel electrode material could decrease the large thermal expansion and reduce the possibility of delamination of the fuel electrode layer from the electrolyte. To investigate the redox reversibility of the Nb_2TiO_7 sample, the powders were further treated in air and then reduced for 3 cycles. As demonstrated in Fig.1 (c) and (d), the XRD patterns correspond to the samples of Nb_2TiO_7 (PDF No.039-1407) and $Nb_{1.33}Ti_{0.67}O_4$ (PDF No.053-0293), respectively. The intensities of the peaks are most likely different because of the difference in the crystalline size and orientation. These results demonstrate the excellent reversibility of Nb_2TiO_7 ceramic

DOI:10.1063/1674-0068/28/cjcp1412210

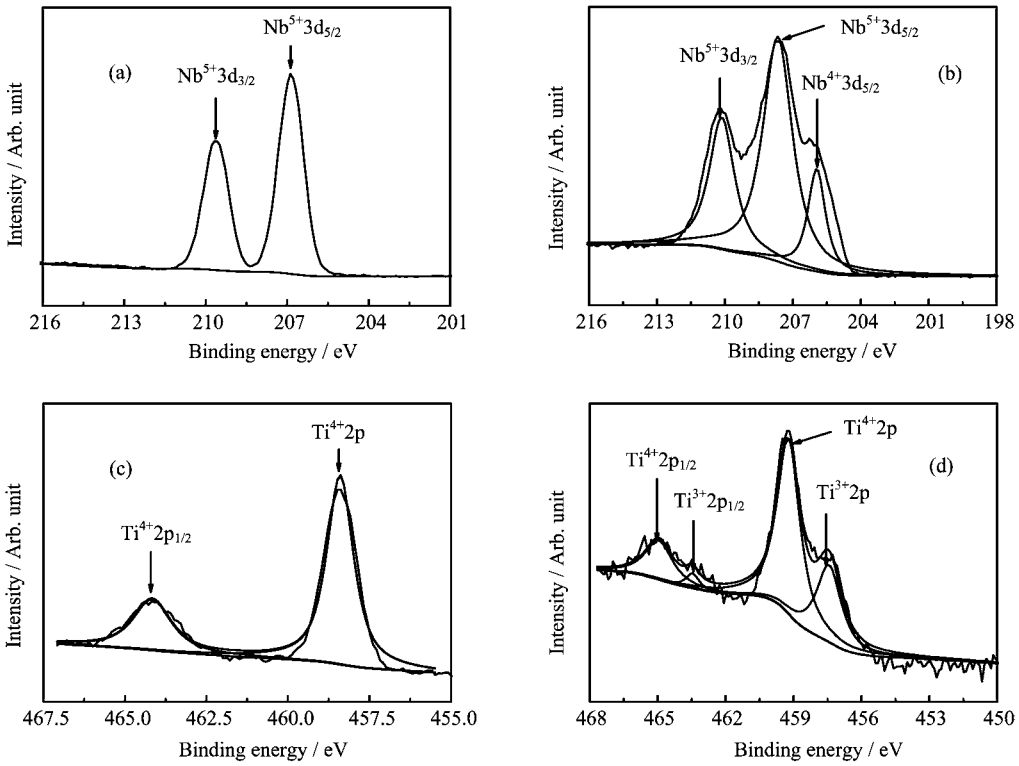

FIG. 2 XPS results of Nb (a) and Ti (c) in Nb_2TiO_7 and Nb (b) and Ti (d) in $Nb_{1.33}Ti_{0.67}O_4$.

powders. The 3-cycle redox tests indicate that composite fuel electrodes based on this ceramic are expected to demonstrate better cycling performances for oxidation and reduction.

To further validate the elemental valence change of Nb_2TiO_7 in the reduced process, XPS was performed to test the oxidized sample Nb_2TiO_7 and the reduced sample $Nb_{1.33}Ti_{0.67}O_4$. As shown in Fig.2(a), only Nb^{5+} is observed in the Nb_2TiO_7 sample [25, 26]. However, the Nb^{5+} is partially reduced into Nb^{4+} [27, 28] in $Nb_{1.33}Ti_{0.67}O_4$, as observed in Fig.2(b). The low valance of Nb ions is favorable for the formation of a Nb−Nb metal bond, and the electronic conductivity is hence highly facilitated [23]. In contrast, the Ti is completely Ti^{4+} in the Nb_2TiO_7 sample [29, 30]. However, low-valence Ti^{3+} is also observed in the reduced sample $Nb_{1.33}Ti_{0.67}O_4$, which is due to the reduction of Ti^{4+} to Ti^{3+} after the heat treatment in reducing gas [31, 32]. The XPS results confirm that the Ti^{4+} and Nb^{5+} can be reduced simultaneously at 830 °C in H_2 atmosphere.

The dependences of the conductivity on the temperature and oxygen partial pressure of Nb_2TiO_7 and the reduced sample $Nb_{1.33}Ti_{0.67}O_4$ were systematically investigated, as shown in Fig.3. The Nb_2TiO_7 is a p-type conductor with an electrical conductivity between 10^{-7} and 10^{-3} S/cm at intermediate temperature in air, as observed in Fig.3(a). However, the conductivity increases gradually upon decreasing the oxygen partial pressure at 800 °C, as observed in Fig.3(b), which may be related to the reduction of the NTO sample in reducing atmosphere. In contrast, the conductivity of the $Nb_{1.33}Ti_{0.67}O_4$ is significantly enhanced to an electronic conductor level, as observed in Fig.3(c), where the conductivity reaches approximately 2−11 S/cm below 400 °C but is further enhanced and finally reaches 39 S/cm at 800 °C in 5%H_2/Ar. The high conductivity of $Nb_{1.33}Ti_{0.67}O_4$ is due to the edge sharing of NbO_6 octahedra along the *c*-axis, producing Nb−Nb metal bond overlap with an intermetallic distance of 0.3 nm. This high electronic conductivity is facilitated by the edge-sharing octahedra along the *c*-axis [23]. As shown in Fig.3(d), the conductivity of $Nb_{1.33}Ti_{0.67}O_4$ gradually decreases upon increasing the oxygen partial pressure, which demonstrates the n-type conductivity property of this material. However, the conductivity of the $Nb_{1.33}Ti_{0.67}O_4$ sample significantly decreases as the sample is oxidized when the oxygen partial pressure is above 10^{-4} atm. NTO is a p-type and n-type mixed conductor. The kink at approximately 450 °C may be related to the combined action of the p-type and n-type electrical conductivity properties, and the n-type conductivity property is dominant.

Figure 4 (a) and (b) show the AC impendence results of the symmetric solid oxide cell with the configuration NTO-SDC/YSZ/NTO-SDC tested at 830 °C with two electrodes exposed to pure H_2 under different passing current densities. The intercept of the impedance spectra with the real axis at high frequency corresponds

DOI:10.1063/1674-0068/28/cjcp1412210

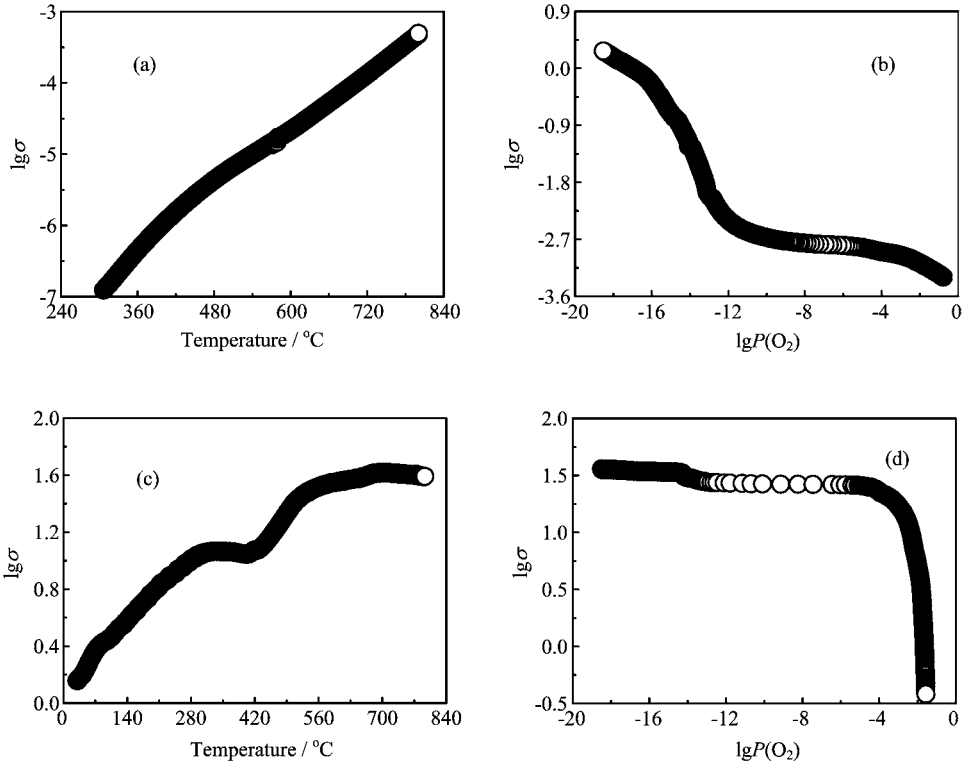

FIG. 3 The electrical conductivity of (a) Nb_2TiO_7 in air and (c) $Nb_{1.33}Ti_{0.67}O_4$ in 5%H_2/Ar, respectively. The dependence of the conductivity of (b) Nb_2TiO_7 and (d) $Nb_{1.33}Ti_{0.67}O_4$ on the oxygen partial pressure at 800 °C.

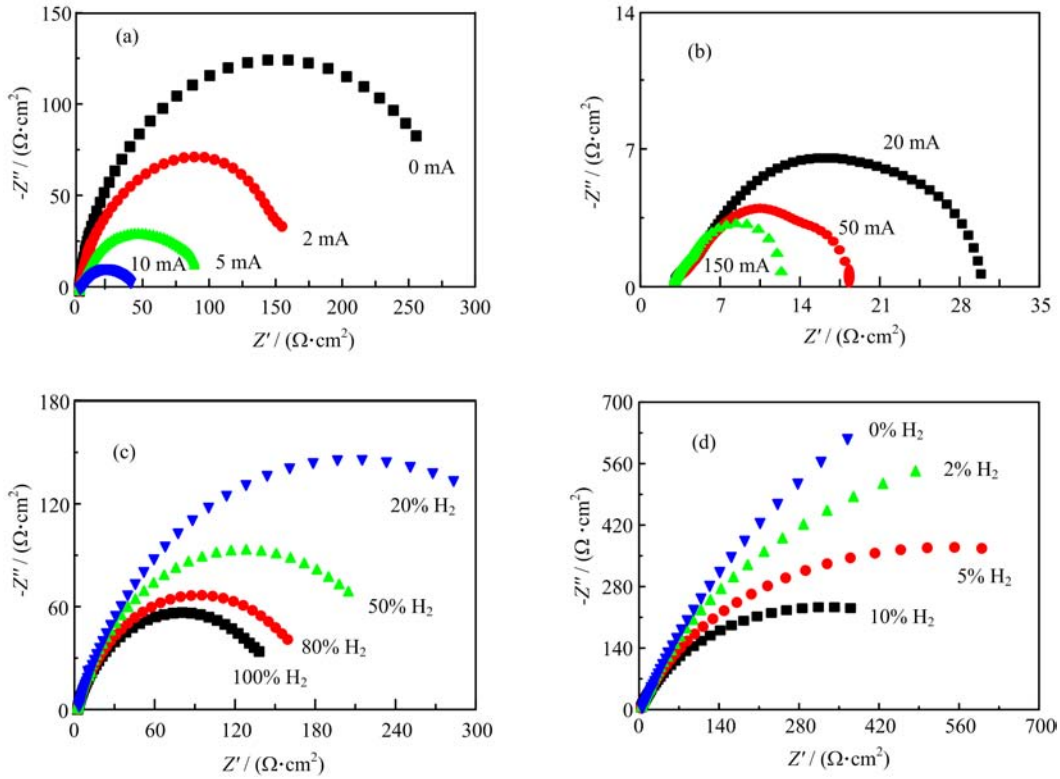

FIG. 4 AC impendence of the symmetric solid oxide cell NTO-SDC/YSZ/NTO-SDC tested at 830 °C with electrodes exposed to (a, b) pure H_2 under different current densities, (c, d) different oxygen partial pressures under the OCV condition.

DOI:10.1063/1674-0068/28/cjcp1412210

to the series resistance of the cell, which mainly results from the ionic resistance of the YSZ electrolyte. The intercept with the real axis at low frequency is considered the total polarization resistance, whereas the difference between the two intercepts is considered the electrode polarization resistance. The series resistance of the symmetric cell is approximately 2.8 $\Omega\cdot cm^2$, which is reasonable for a 2-mm-thick YSZ electrolyte at 830 °C. The electrode polarization resistance is approximately 300 $\Omega\cdot cm^2$ under low-current-passing electrodes; however, polarization resistance decreases to only approximately 10 $\Omega\cdot cm^2$ with 150-mA current-passing electrodes, which demonstrates the sufficient activity of the $Nb_{1.33}Ti_{0.67}O_4$ electrode under different current densities in H_2. Figure 4 (c) and (d) present the AC impendence results of the symmetric solid oxide cell tested at 830 °C with two electrodes exposed to different hydrogen partial pressures under the OCV condition. The electrode polarization resistance of the symmetric cell is approximately 160 $\Omega\cdot cm^2$ under pure hydrogen atmosphere and gradually increases upon decreasing the hydrogen partial pressure, which is closely related to the n-type conducting properties of the $Nb_{1.33}Ti_{0.67}O_4$ ceramic.

Figure 5 shows the microstructure of the electrolyte-supported SOE with the configuration NTO-SDC/YSZ/LSM-SDC. The two porous electrodes with thicknesses of approximately 20 μm are observed to adhere to the electrolyte very well. The current collector layer is approximately 5 μm in thickness. The NTO-SDC composite electrode matches well with the YSZ electrolyte.

To verify the sealing of the single SOE with the configuration NTO-SDC/YSZ/LSM-SDC, the OCV was recorded with $3\%H_2O/Ar/4\%H_2$ fed to the fuel electrode, and the oxygen electrode exposed to static air. The OCV reaches 0.91 V, which indicates good separation between the anodic and cathodic gas. Figure 6(a) presents the *I-V* curve of the electrolyzer at 830 °C with $4\%H_2/Ar/3\%H_2O$ introduced to the fuel electrode and the oxygen electrode exposed to static air. The relationship between the current and applied voltage is far from linear with the maximum current density reaching 98 mA/cm^2 at 2 V. To study the change of the electrolyzer resistance under different voltages, the dV/dI curves (cell resistance) were plotted versus voltage, as shown in Fig.6(b). The cell resistance significantly drops above 0.9 V. However, it is generally stable above 1.5 V. It was therefore concluded that there may be different dominant processes in this voltage region. The cell resistance sharply decreases as a function of the applied voltage from the OCV (0.91 V) to 2.0 V, which is most likely attributed to the reduction and activation of the NTO composite fuel electrode. However, the higher voltage improves the electrode reactions, which would further enhance the electrode electrochemical process and decrease the electrode polarization resistance at higher voltages.

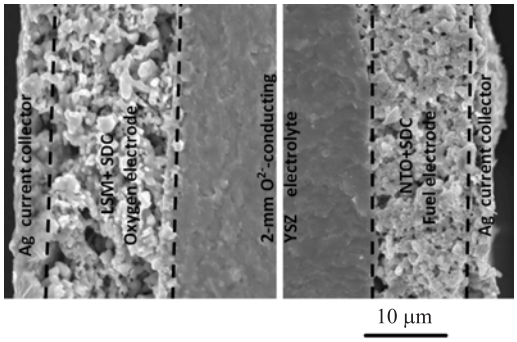

FIG. 5 Microstructure of the SOE with the configuration NTO-SDC/YSZ/LSM-SDC.

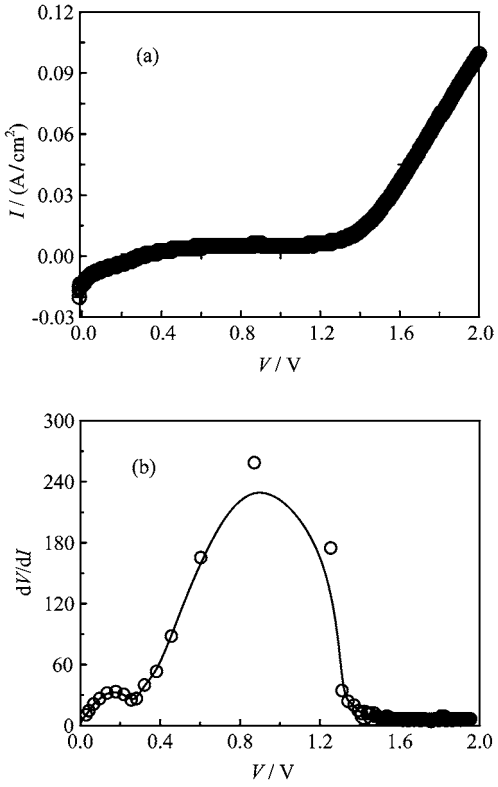

FIG. 6 (a) *I-V* curve and (b) dV/dI (cell resistance) of the SOE NTO-SDC/YSZ/LSM-SDC tested at 830 °C with $3\%H_2O/Ar/4\%H_2$ fed to the fuel electrode and the oxygen electrode exposed to static air.

Figure 7(a) plots the current density versus time and the applied voltage of the electrolyzer tested at 830 °C with $4\%H_2/Ar/3\%H_2O$ fed into the fuel electrode and the oxygen electrode exposed to static air. The current density reached approximately 5, 7, 21, 66, and 80 mA/cm^2 at 1.1, 1.3, 1.5, 1.8, and 2.0 V, respectively. As observed in Fig.7(b), the productions of H_2 are 1.4, 13.4, 13.4, 432.0, and 556.0 $\mu L/(min\cdot cm^2)$ at 1.1, 1.3, 1.5, 1.8, and 2.0 V, respectively. The corresponding current efficiencies are 4.0%, 30.5%, 84.8%, 98.4%, and 98.9%, respectively. The performance of

DOI:10.1063/1674-0068/28/cjcp1412210

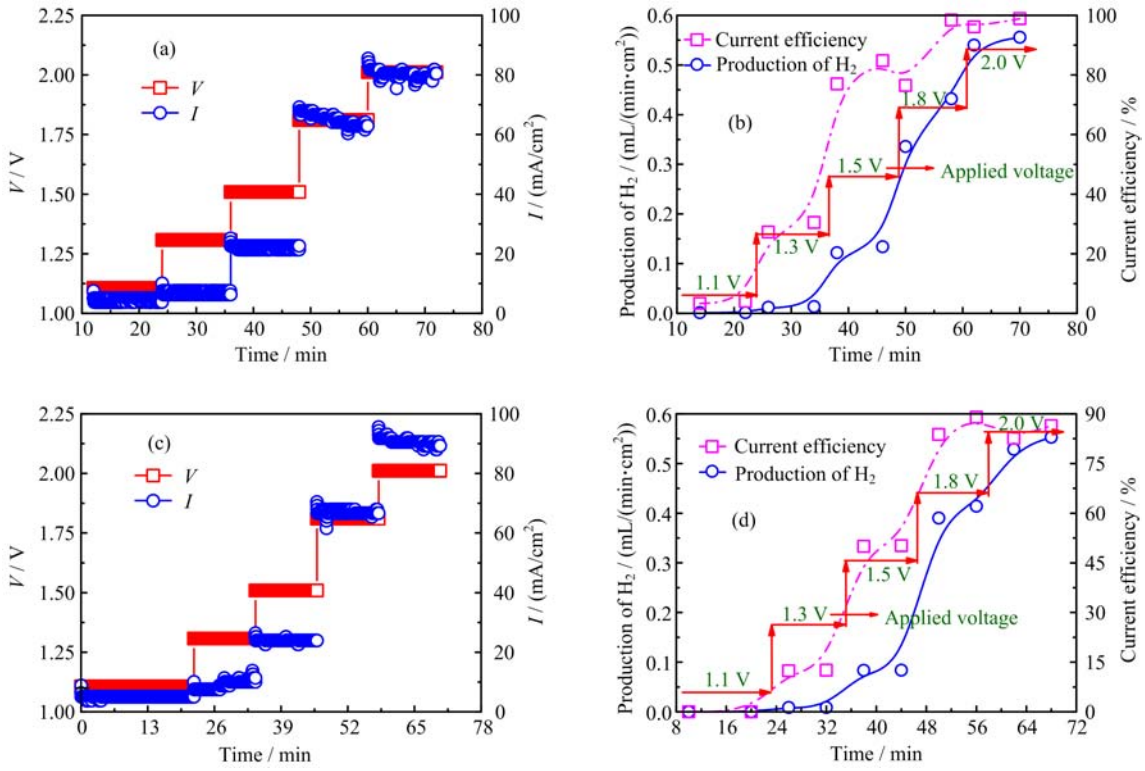

FIG. 7 (a, c) Short-term performance and (b, d) production of H_2 and current efficiency of the SOE NTO-SDC/YSZ/LSM-SDC tested at 830 °C with 3%H_2O/Ar/4%H_2 and 3%H_2O/Ar fed to the fuel electrode and the oxygen electrode exposed to static air, respectively.

the steam electrolysis based on the NTO electrode electrolyzer is much better than that reported for the $La_{0.75}Sr_{0.25}Cr_{0.5}Mn_{0.5}O_{3-\delta}$ electrode electrolyzer [24].

There are two main electrochemical processes in the range from the OCV to 2 V during the steam electrolysis process: the reduction and activation of the NTO electrode and steam electrolysis. The reduction and activation of NTO is the main process below 1.5 V, whereas the electrochemical reduction of H_2O mainly dominates the electrolysis process at high voltage. Figure 6(b) shows that the dV/dI (cell resistance) is approximately 6 $\Omega\cdot cm^2$ above 1.5 V and remains constant, which indicates the sufficient reduction and activation of the fuel electrode and a stable steam electrolysis process.

Figure 7(c) plots the current density versus time and the applied voltage of the electrolyzer direct steam electrolysis (3%H_2O/Ar) without reducing gas flow over the fuel electrode. The current density reached approximately 5, 11, 23, 66, and 91 mA/cm^2 at 1.1, 1.3, 1.5, 1.8, and 2.0 V, respectively. As observed in Fig.7(d), the productions of H_2 are 8.8, 83.8, 414.0, and 552.7 μL/(min·cm^2) at 1.3, 1.5, 1.8, and 2.0 V, respectively. The corresponding current efficiencies are 12.6%, 50.2%, 89%, and 86.4%, respectively. The lower efficiencies under low voltage and high efficiencies under high voltages are related to the reduction, and the activation of NTO is the main process below 1.5 V, whereas the electrochemical reduction of H_2O mainly dominates the electrolysis process at high voltage. The electrolysis current efficiency decreased without H_2 in the feeding gas, which may be related to the decreasing of the electrode catalytic performance in lower reduced atmosphere. The current efficiencies of the electrolyzer for direct steam electrolysis are comparable to that of the electrolyzer based on a $La_{0.2}Sr_{0.8}TiO_{3+\delta}$ composite fuel electrode [13]. These electrolysis results indicated that a high-temperature SOE with Nb_2TiO_7 composite electrode can be operated in an atmosphere without H_2 for steam electrolysis.

IV. CONCLUSION

In this work, a composite fuel electrode based on Nb_2TiO_7 was investigated in an oxide-ion-conducting SOE with YSZ electrolyte support. The dependence of the conductivity of Nb_2TiO_7 and reduced $Nb_{1.33}Ti_{0.67}O_4$ on the temperature and oxygen partial pressure were investigated and correlated with the electrochemical properties of the electrode. A SOE for steam electrolysis was prepared and electrochemically studied at 830 °C based on the composite $Nb_{1.33}Ti_{0.67}O_4$ fuel electrode. The short-term performance tests indicate that the steam electrolysis process is stable and that the maximum current efficiency of

DOI:10.1063/1674-0068/28/cjcp1412210

the electrolyzer reaches 98.9% with 3%H_2O/Ar/4%H_2 fed into the fuel electrode and 89% using 3%H_2O/Ar. The results indicated that Nb_2TiO_7 might be a candidate for the fuel electrode (cathode) material of high-temperature SOEs in atmosphere with low content of H_2 or without H_2.

[1] A. Brisse, J. Schefold, and M. Zahid, Int. J. Hydrogen Energy **33**, 5375 (2008).
[2] A. Hauch, S. Ebbesen, S. Jensen, and M. Mogensen, J. Mater. Chem. **18**, 2331 (2008).
[3] G. Schiller, A. Ansar, M. Lang, and O. Patz, J. Appl. Electrochem. **39**, 293 (2009).
[4] C. Jin, C. Yang, F. Zhao, D. Cui, and F. L. Chen, Int. J. Hydrogen Energy **36**, 3340 (2011).
[5] A. Ursua, L. M. Gandia, and P. Sanchis, Proc. IEEE **100**, 410 (2012).
[6] K. Xie, Y. Q. Zhang, G. Y. Meng, and J. T. S. Irvine, Energ. Environ. Sci. **4**, 2218 (2011).
[7] K. Xie, Y. Q. Zhang, G. Y. Meng, and J. T. S. Irvine, J. Mater. Chem. **21**, 195 (2011).
[8] W. Doenitz, R. Schmidberger, E. Steinheil, and R. Streicher, Int. J. Hydrogen Energy **5**, 55 (1980).
[9] W. Balthasar, Int. J. Hydrogen Energy **9**, 649 (1984).
[10] S. Dutta, Int. J Hydrogen Energy **15**, 379 (1990).
[11] X. Yang and J. T. S. Irvine, J. Mater. Chem. **18**, 2349 (2008).
[12] M. Ni, M. K. H. Leung, and D. Y. C. Leung, Int. J. Hydrogen Energy **33**, 2337 (2008).
[13] S. S. Li, Y. Li, Y. Gan, K. Xie, and G. Meng, J. Power Sources **218**, 244 (2012).
[14] F. Bidrawn, G. Kim, G. Corre, J. T. S. Irvine, J. M. Vohs, and R. J. Gorte, Electrochem. Solid State Lett. **11**, B167 (2008).
[15] M. Bossche and S. McIntosh, Chem. Mater. **22**, 5856 (2010).
[16] S. W. Tao, J. T. S. Irvine, and J. A. Kilner, Adv. Mater. **17**, 1734 (2005).
[17] D. M. Bastidas, S. W. Tao, and J. T. S. Irvine, J. Mater. Chem. **16**, 1603 (2006).
[18] S. W. Tao and J. T. S. Irvine, Nature Mater. **2**, 320 (2003).
[19] Y. Gan, J. Zhang, Y. X. Li, S. S. Li, K. Xie, and J. T. S. Irvine, J. Electrochem. Soc. **159**, F1 (2012).
[20] S. W. Tao and J. T. S. Irvine, J. Electrochem. Soc. **151**, A252 (2004).
[21] K. Xie, Y. Q. Zhang, G. Y. Meng, and J. T. S. Irvine, Energ. Environ. Sci. 4, 2218 (2011).
[22] G. Tsekouras, D. Neagu, and J. T. S. Irvine, Energ. Environ. Sci. **6**, 256 (2013).
[23] A. Lashtabeg, J. C. Vazquez, J. T. S. Irvine, and J. L. Bradley, Chem. Mater. **21**, 3549 (2009).
[24] S. S. Xu, S. Chen, M. Li, K. Xie, Y. Wang, and Y. Wu, J. Power Sources **239**, 332 (2013).
[25] R. Fontaine, R. Caillat, L. Feve, and M. J. Guittet, J. Electron Spectrosc. Relat. Phenom. **10**, 349 (1977).
[26] A. Darlinski and Halbritter, J. Surf. Interface Anal. **10**, 223 (1987).
[27] M. K. Bahl, J. Phys. Chem. Solids **36**, 485 (1975).
[28] R. Fontaine, R. Caillat, L. Feve, and M. J. Guittet, J. Electron Spectrosc. Relat. Phenom. **10**, 349 (1977).
[29] F. Lange, H. Schmelz, and H. Knozinger, J. Electron Spectrosc. Relat. Phenom. **57**, 307 (1991).
[30] A. R. Burke, C. R. Brown, W. C. Bowling, J. E. Glaub, D. Kapsch, C. M. Love, R. B. Whitaker, and W. E. Moddeman, Surf. Interface Anal. **11**, 353 (1988).
[31] A. R. Chourasia and D. R. Chopra, Surf. Sci. Spectra **1**, 233 (1992).
[32] S. Badrinarayanan, S. Sinha, and A. B. Mandale, J. Electron Spectrosc. Relat. Phemon. **49**, 303 (1989).

DOI:10.1063/1674-0068/28/cjcp1412210